Oxidation of Metals, Vol. 11, No. 4, 1977

The Isothermal Oxidation of Co–Cr Alloys in 760 Torr Oxygen at 1000°C

I. G. Wright*† and G. C. Wood*

Received February 16, 1977

The isothermal oxidation of Co–Cr alloys containing 0–30% Cr in 760 Torr oxygen at 1000°C has been studied kinetically and by appropriate physical techniques. Chromium additions to cobalt increase the parabolic oxidation rate to an almost constant level from 2 to 15% Cr, while further additions to 20–30% Cr decrease the rate. All the alloys produce a virtually pure CoO layer outside a layer containing Co–Cr spinel particles in a Cr^{3+}-doped CoO matrix. The variation of oxidation rate with alloy chromium content is explained in terms of the complex interplay of doping, blocking of cation transport by voids and spinel particles and short circuiting by transport of dissociative oxygen across these voids and other processes, internal oxidation making a negligible direct contribution to weight gain. Complete spinel layers are never quite developed under the conditions studied, although formation of spinel does slow the oxidation rate. The improved protection eventually obtained at higher chromium levels is produced by the tendency to form a Cr_2O_3 healing layer.

KEY WORDS: cobalt–chromium; oxidation; oxygen.

INTRODUCTION

Improvements in gas turbine performance and efficiency have required ever-increasing operating temperatures and therefore have made progressively more severe demands on the materials of construction. There have been much experimentation and discussion in recent years regarding the

*Corrosion and Protection Centre, University of Manchester Institute of Science and Technology, Manchester, England.
†Battelle-Columbus Laboratories, Columbus, Ohio.

relative hot strength, creep resistance, and high-temperature oxidation and hot-corrosion resistance of alloys based on the Co–Cr and Ni–Cr systems. Curiously, relatively little work has been published on fundamental understanding of the high-temperature oxidation of pure Co–Cr alloys themselves. Following early studies in which kinetic considerations predominated,[1–3] only two groups [5–8,9–12] have undertaken independent detailed studies, with a third[13,14] investigating Co–Cr alloys incidentally with a major aim of examining the influence of ternary additions. Effort has been directed principally at understanding the reasons why small chromium additions increase the oxidation rate of cobalt[5,6,8,9–12] and the difficulty in establishing and maintaining a protective Cr_2O_3 scale on the alloys,[5,7,9,10,12] and in making comparisons between the oxidation behaviors of corresponding Ni–Cr and Co–Cr alloys.[9–11]

The present paper describes a systematic study of the oxidation of Co–Cr alloys from various sources, containing 0–30% Cr, mainly at 1000°C and 760 Torr of oxygen. Particular emphasis is placed on investigation by optical and scanning electron microscopy, aided by electron probe microanalysis.

EXPERIMENTAL PROCEDURE

The 11 alloys were obtained from four different sources; their nominal and chemical analyses and the purities of the starting materials are given in Table I. Batch A was obtained in the form of small ingots, which were then cut into slices by spark machining, sawing, and grinding. With Batch B, a poor arc-melting technique led to the entrapping of numerous Cr_2O_3 particles inside the ingots, which were themselves converted to slices by spark machining, etc. Batch C was made by induction melting, vacuum casting, and hot rolling to 0.22 cm. Finally, batch D was prepared by vacuum melting and casting and then hot-rolling, followed by surface grinding to 0.18 cm thickness. The thick strips of batches C and D were cold rolled to a final thickness of 0.05 cm at approximately 0.003 cm reduction per pass, with intermediate 4 hr vacuum anneals at 1000°C after each 0.025 cm reduction.

Prior to oxidation, specimens were typically ground (ingot slices) or cold sheared to approximately 2.0×0.5 cm, drilled to accept the suspension wire, polished on 600 grade SiC paper, degreased in trichlorethylene, and annealed at 1000°C for 5 hr at 2×10^{-5} Torr or better. They were then electropolished in a glacial acetic acid–perchloric acid–water mixture[12] immediately prior to oxidation, yielding a surface which was smooth, with little pitting, but undulating on a small scale. These electropolished specimens were then cathodically etched in 5 vol.% HF until an active surface was just produced, and then washed. A few abraded specimens were also studied.

Table I. Analysis of Co–Cr Alloys and Starting Materials

Nominal analysis, wt.%	Wet chemical analysis, wt.% Cr	Analysis of cobalt starting material, impurities, ppm	Analysis of chromium starting material, impurities, ppm
Batch A			
Co	—	99.999% Co	99.995% iodide Cr
Co–1Cr	0.979		
Co–2Cr	1.95	(Si 3; Fe 2; Al,	(O 8; Ni, H, Mg 1;
Co–5Cr	5.21	Ca, Cu, Mg 1;	N 3; C, Si 10;
Co–15Cr	14.93	Ag < 1)	Al 1–2; Ca 2;
Co–30Cr	30.3		Cu 1–10, Fe 2–16;
			V 0.3)
Batch B			
Co–5Cr	—	99.99% Co sponge	(N 7; C 50; O 350;
		(Ca 1; Cu 5; Fe 10;	H 100; Pb 3;
		Ni 30; Si 5; Na 1;	Sn, Al, Na 4;
		Mg and Ag < 1)	Fe 3; Mg, Cu, Ni,
			Ag, Sb, Bi < 1)
Batch C			
Co–20Cr	20.3	99.999% Co	99.999% Cr
Batch D			
Co–10Cr	10.1	Electrolytic Co	99.9% Cr
Co–30 Cr	29.0	(C 20; S 10; Fe 58;	
		Cu 25; Ni 600;	
		Zn 80; Si 10; Mn 1;	
		P 30; H 2; O 31)	

Oxidation was performed in a silica spring thermobalance,[15] the specimens being rapidly lowered into the oxygen–flushed hot zone. Oxygen of 99.5% analysis (CO_2 5 ppm, hydrocarbons 10 ppm, H 50 ppm, Ar 0.5%, N trace, water vapor $< 0.15\ g \cdot m^{-3}$) was purified further by passage through magnesium perchlorate, phosphorus pentoxide, and sulfuric acid and directed at $15\ ml \cdot min^{-1}$ through the apparatus. Runs were terminated by winching the specimen out of the hot zone over a 10 min period to minimize scale loss.

RESULTS

Kinetics

The weight gain vs time data obtained for each of the four to eight specimens per alloy oxidized were plotted on log–log coordinates, and the oxidation rate index n was determined, assuming the kinetics to have the

form $w^n = kt$, where w is the weight gain, k is a constant, and t is the time. For pure cobalt n was 2.0 through the exposure period, indicating that the oxidation was parabolic with no deviations (Table II). Reproducibility from specimen to specimen was excellent, being independent of the surface finishes employed and specimen shape, and the results agreed well with literature values.

The oxidation kinetics of all the alloys containing 1–30% Cr were generally self-consistent and very similar from alloy to alloy (Fig. 1a–d). Various batches of specimens which had been heavily abraded, or annealed and abraded, or hot rolled and abraded, produced results essentially identical to those with the standard pretreatment. Significant scatter was observed in the weight gain/time curves for Co–1% Cr and Co–2% Cr, the results for Co–2% Cr occupying the band in Fig. 1a, while those of Co–1% Cr occupied a similar band extending to slightly lower weight gains. The reproducibility of the Co–5, –10, and –15% Cr alloys was very much better than this (Fig. 1b). Co–1, –10, and –15% Cr alloys followed a single rate law throughout the

Table II. Kinetics of Co–Cr Alloys in Oxygen at 1000°C

Alloy	Value of rate index n	Range of application, $mg \cdot cm^{-2}$		k_p, $g^2 \cdot cm^{-4} \cdot sec^{-1}$
		n	k_p	
Pure Co	2.0	0–max	0–max	2.1×10^{-8}
Co–1% Cr	1.7–1.9	2–max	0–7	3.0×10^{-8}
			8–max	4.0×10^{-8}
Co–2% Cr	1.4–1.7	0–12	0–max	4.4×10^{-8}
	1.8–2.1	12–max		
Co–5% Cr	1.0	0–3		
	1.7–1.8	3–max	0–19	4.5×10^{-8}
			19–max	5.5×10^{-8}
Co–5% Cr	1.0	0–5		3.8×10^{-8}
(Batch B)	1.8	5–max	0–10	4.1×10^{-8}
			10–max	
Co–10% Cr	1.7–1.9	0–max	0–max	5.4×10^{-8}
Co–15% Cr	1.9	3–max	0–max	4.3×10^{-8}
Co–20% Cr	2.4–2.5	0–28	0–10	1.2×10^{-8}
(Batch C)	2.9	28–max	10–max	4.8×10^{-9}
Co–30% Cr	1.9–2.3	0–3		
	1.4–1.8	3–max	3–19	3.6×10^{-9}
			19–max	5.4×10^{-9}
Co–30% Cr[a]	1.5	0–3	0–6	$\sim 5.0 \times 10^{-10}$
(Batch D)	2.2	3–max	6–max	$\sim 4.6 \times 10^{-10}$

[a] Abraded specimens only.

exposure period (Table II), the rate index being 1.7 to 1.9, whereas the initial stages of oxidation of Co–2%Cr (up to 1 hr), Co–5%Cr (up to 20 min), and batch D Co–30%Cr (up to 5 hr) alloys gave values of n in the range 1.0 to 1.7. In the subsequent periods of oxidation n assumed a value nearer that denoting parabolic behavior (1.7 to 2.2).

The oxidation kinetics of Co–20%Cr were quite reproducible (Fig. 1c) and yet the value of the rate index was around 2.5, approaching 2.9 with long

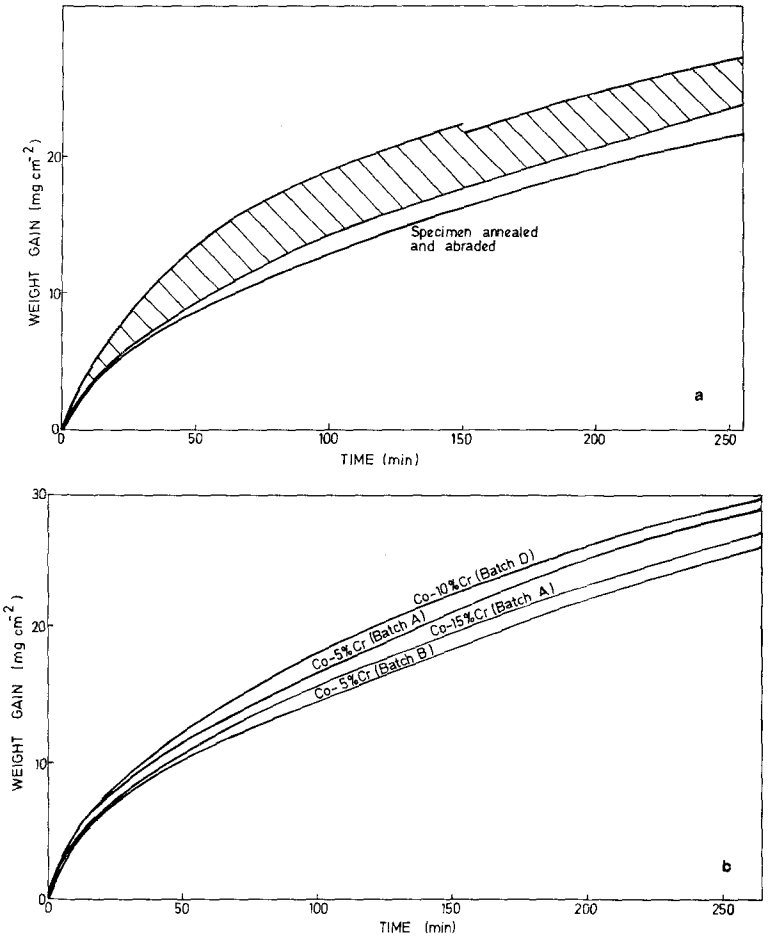

Fig. 1. Weight gain–time curves for the oxidation of Co–Cr alloys in 760 Torr oxygen at 1000°C. (a) Co–2%Cr (batch A). The curves for various specimens, which were either annealed, abraded, electropolished, and then etched, or annealed, etched, electropolished, and then etched, all lay within the hatched band, the boundaries of which are individual growth curves. (b) Co–5%Cr (batches A and B), Co–10%Cr (batch D) and Co–15%Cr (batch A).

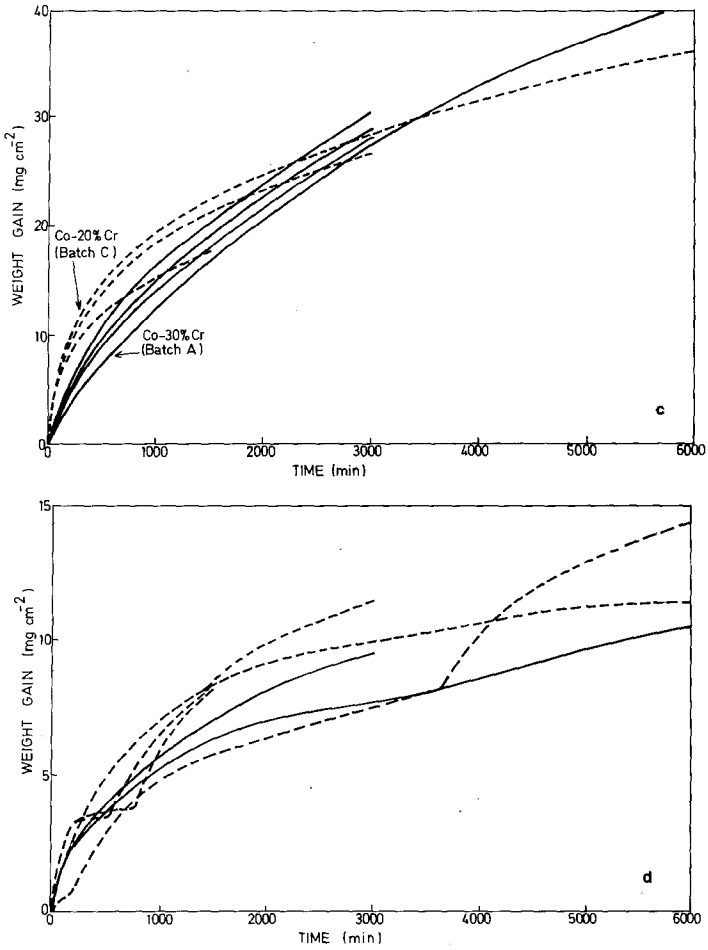

Fig. 1. Continued. (c) Co–20%Cr (batch C) and Co–30%Cr (batch A). (d) Co–30%Cr (batch D). Full curves refer to specimens which were annealed and abraded; dotted curves apply to annealed, electropolished and then etched specimens.

exposure time (> 50 hr). Batch A Co–30%Cr gave reasonably reproducible but quite complex kinetic curves (Fig. 1c). After an initial incubation period of up to 2 hr, during which the oxidation rate was very slow and parabolic, the rate increased and obeyed a rate law faster than parabolic ($n = 1.5$) up to a weight gain of 12–15 mg · cm^{-2}. After this the rate again increased while the rate law became nearer parabolic.

Annealed and abraded specimens of batch D Co–30%Cr oxidized parabolically or faster ($n = 2.0$ to 2.5), while annealed, electropolished, and

etched specimens oxidized with random surges of fast oxidation (Fig. 1d), resulting in locally thick areas of oxide.

For comparison purposes approximate parabolic rate constants were obtained by drawing the best straight line (or lines) through the data for each specimen when plotted as weight gain squared against time coordinates. The values listed in Table II are the averages of the constants of several specimens oxidized. In the parabolic plots for Co–1 to –15% Cr the experimental points for each specimen lay accurately on a straight line in areas where log–log plots had indicated the rate was parabolic. Least squares plots etc. were used where appropriate.

Plots of the average parabolic rate constants for Co–0 to –15% Cr alloys and approximate parabolic rate constants for Co–20 and –30% Cr against chromium content (Fig. 2) illustrate that Co–1 to –15% Cr alloys all oxidized faster than pure cobalt, while the oxidation rate decreased rapidly as the chromium level increased with Co–20 and –30% Cr. However, compared

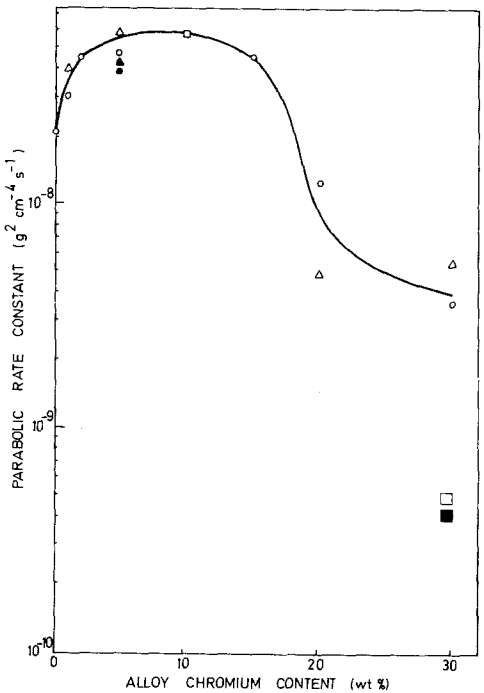

Fig. 2. Parabolic rate constant for the oxidation of Co–Cr alloys in 760 Torr oxygen at 1000°C as a function of alloy chromium content. (○) Initial rate, (△) final rate, batch A and C alloys. (●), (▲) Batch B alloy. (□) Initial rate, (■) final rate, batch D alloys.

with the results of Phalnikar *et al.*[2] in air, no sharp maximum or minimum in oxidation rate was found in the 9 and 26% Cr regions, respectively.

Scale Morphology and Structure

The dark gray, outer surface of the scales showed characteristic, often equiaxed and sometimes straight-sided, faceted grains, with subgrain boundaries decorated by Co_3O_4 standing proud. The grain size on the outer surface increased with time for all the alloys, the grain size being roughly the same after 5 hr for cobalt and alloys up to Co–15% Cr, while that of Co–20% Cr was much smaller. For shorter oxidation times the grain size on Co–1 and –2% Cr appeared to be larger than on cobalt and the other alloys. The ratio of grain depth to width remained roughly constant at 0.86 to 1.6 for all times and alloys.

Cobalt

The scales formed on cobalt were uniformly thick on all the sides and were relatively compact (Fig. 3a). Much of the gross porosity apparent in the columnar grains was shown (Fig. 3c–e) to have resulted from metallographic preparation, although the fine porosity near the metal surface was probably genuine. Most of the scale was tightly adherent to the metal, only slight separation occurring in places on cooling. A very thin layer of small almost equiaxed grains was evident at the base of the flat-topped columnar oxide, which retained approximately the same proportionate thickness to the columnar grains (1 : 25) as the total scale thickened. At the specimen corners the proportion of columnar to small-grained oxide reached a minimum, while the total scale thickness was slightly greater than on the flat sides (Fig. 3b,c).

The fracture pattern of the fine-grained oxide, when compared with that of the columnar oxide (Fig. 3), suggested the possibility of a porous network near the metal surface and a relatively sharp transition between the compact columnar grains outside and the small-grained inner layer. The grain size of the inner layer decreased as the metal surface was approached (Fig. 3d,e) until it was very small indeed.

Cobalt–1 to –15% Chromium

The scales on the Co–1 to –10% Cr alloys were all intact after cooling from the test temperature but had parted from the alloy more than on cobalt. In contrast, the scales on Co–15% Cr frequently spalled on cooling. Typical areas of the scales are shown in Figs. 4–6. All were double-layered, decorated with Co_3O_4 as for the scales on cobalt (Fig. 3), and had the inner layer thicker than the outer layer at specimen corners. Although, at first

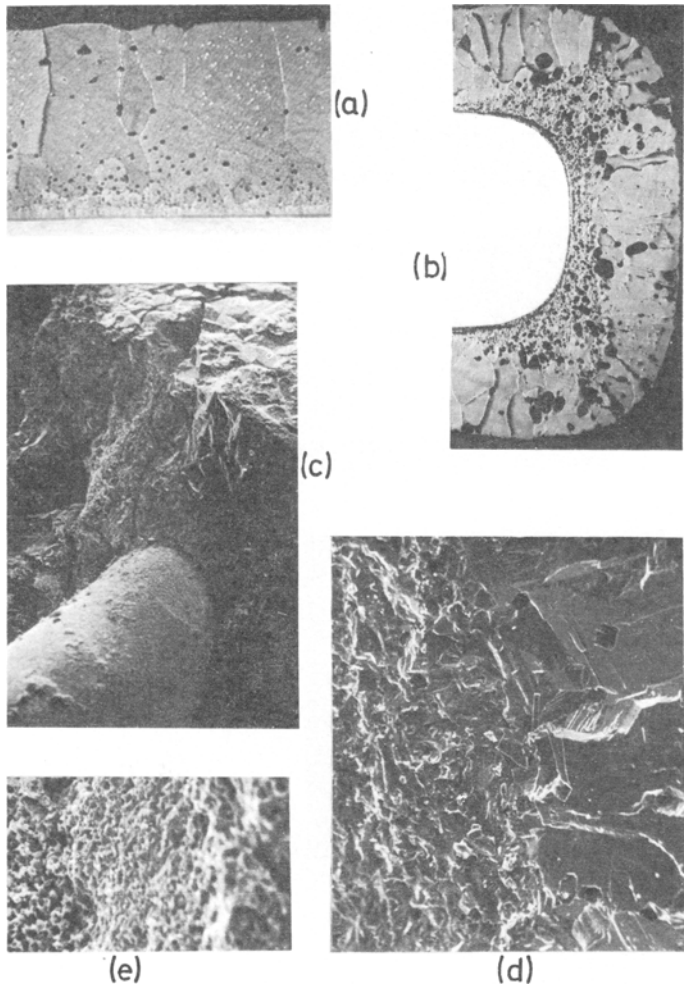

Fig. 3. Micrographs of scales formed on cobalt in 760 Torr oxygen at 1000°C. Optical micrographs of polished sections of scale. (a) Side after 5 hr, ×200; (b) end after 25 hr, ×50. Scanning electron micrographs of fracture sections of 25 hr specimens. (c) General view of metal core with attached oxide, ×58; (d) detail of columnar–fine-grained interface, × 230; (e) fine-grained inner-oxide layer (right-hand side) adherent to metal surface, ×570. All parts reduced 20% for reproduction.

sight at least, the shape and thickness of the inner layer on Co–5, –10, and –15% Cr suggested that it occupied the space vacated by the consumed metal, the inner–outer oxide boundary apparently marking the original gas–metal interface, this semblance did not apply to Co–1 and –2% Cr. Close

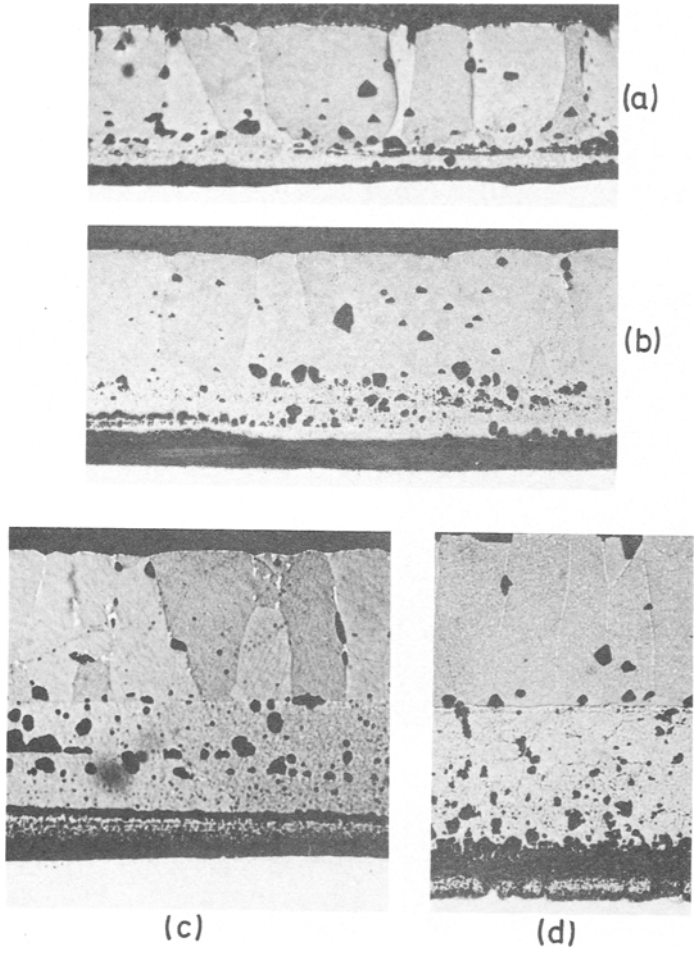

Fig. 4. Optical micrographs of scales formed on Co–1 to –10%Cr alloys in 760 Torr oxygen at 1000°C. (a) Co–1%Cr, 2.5 hr, ×200; (b) Co–2%Cr, 5 hr, ×180; (c) Co–5%Cr, 5 hr, ×200; (d) Co–10%Cr, 5 hr, ×200. All parts reduced 20% for reproduction.

examination of the alloy–oxide interface revealed no significant evidence of internal oxide particles for Co–1, –2, and –5%Cr. A few were found with Co–10%Cr (Fig. 5d), which appeared red in reflected light, indicating a spinel type structure, but penetrating only 3 μ into the alloy after 5 hr. A uniform layer of densely packed internal oxide particles formed on Co–15%Cr (Fig. 5e), this being 4.1, 4.7, 6.4, and 4.7 μ thick after 1, 2.5, 5, and 17 hr, respectively.

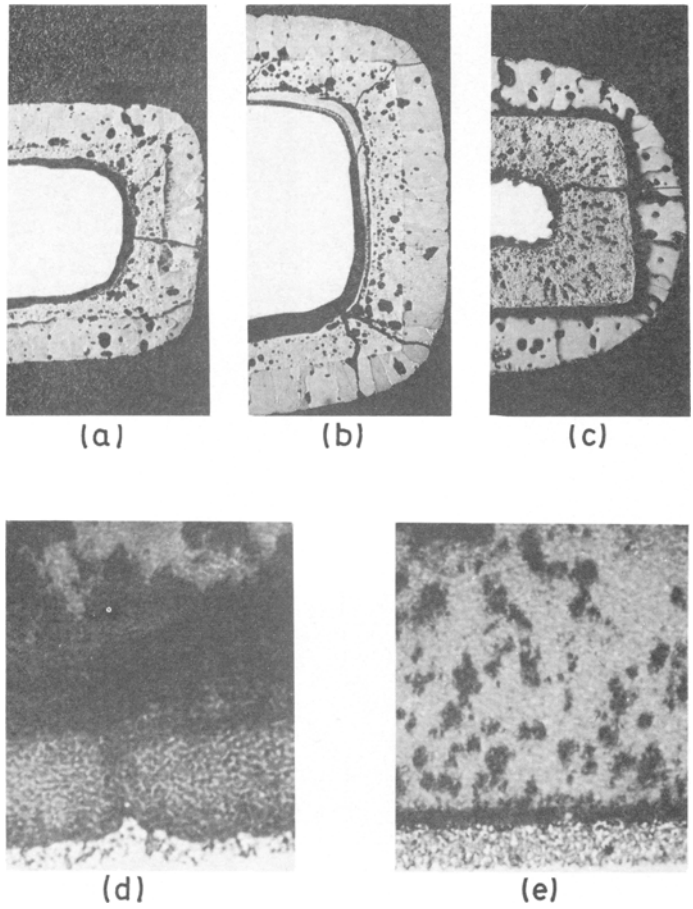

Fig. 5. Optical micrographs of scale growth on specimen ends under conditions of Fig. 4. (a) Co–1%Cr, 5 hr, ×50; (b) Co–5%Cr, 5 hr, ×60; (c) Co–15%Cr, 15 hr, ×50. Detail of the alloy–oxide interface, including internal oxide. (d) Co–10%Cr, 5 hr, ×1000; (e) Co–15%Cr, 5 hr, ×1000. All parts reduced 20% for reproduction.

Much of the porosity apparent in the outer layers of oxide in the photomicrographs was shown to be associated with metallographic preparation, but that in the inner layers appeared genuine. No evidence of banding of the inner layers (Fig. 4a–c) was observed on scanned fracture sections. If such banding was genuine it was presumably due to the scale successively lifting and cracking open at temperature, or to intermittent effects in the internal oxide. Indeed, the similarity in distribution of internal oxide in the alloy and of precipitate in the scale inner layer confirmed that the latter

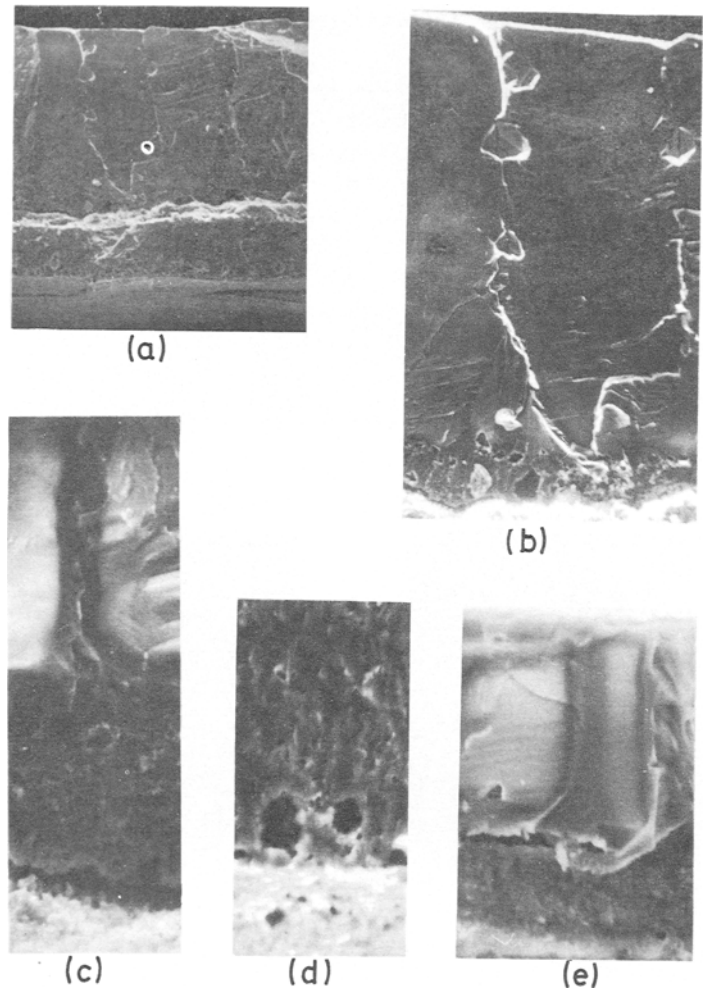

Fig. 6. Scanning electron micrographs of scales formed on Co–2 and –10%Cr alloys in 760 Torr oxygen at 1000°C. (a)–(d) Co–2%Cr, 5 hr. (a) General view of the fracture, ×190; (b) columnar layer, ×495; (c) porosity at the base of the columnar layer, ×1990; (d) inner layer only, ×1990; (e) Co–10%Cr, 15 min, showing the detail of the lifted scale, ×2500. All parts reduced 20% for reproduction.

derived from the former by incorporation in the encroaching scale. Alloys from different sources behaved in the same manner.

In particular, when the polished section of scale formed after 5 hr on Co–2%Cr (Fig. 4b) was compared with the fracture (Fig. 6a), there was a greatly reduced pore population in the columnar oxide of the latter. The few

pores that were observed did, however, have the same triangular shape as in the cross section (Fig. 6b), while a similar configuration was also sometimes seen in the fracture pattern at most columnar grain boundaries. The generally dense outer layer contrasted sharply with the inner layer, which exhibited a fibrous, probably porous fracture pattern (Fig. 6c) and definite fine porosity near the alloy–oxide interface (Fig. 6d). The grain boundaries between the columnar grains appeared free from obvious porosity, except perhaps near the inner layer (Fig. 6d).

Fracture sections of scales on Co–10% Cr showed essentially the same features, with even fewer obvious pores but more triangular facets in the columnar oxide (Fig. 6e) and, in this case, definite horizontal voids at the interface between the two layers (Fig. 6e). Kofstad and Hed[5] claimed that these triangular pores were caused by mechanical shear and deformation. The undulating underside of the blue-colored scale in contact with the alloy had a grain size and structure similar to the alloy viewed in plan. The approximate grain size was 5 μ, compared with 10–20 μ for the inner layer after 5 hr oxidation (Fig. 5a).

A few of the large holes in the columnar CoO were outlined by the lighter Co_3O_4, suggesting that they contained oxygen at temperature, Co_3O_4 precipitating from the oxygen-rich CoO on cooling. Whether the nondecorated voids were artifacts or whether the oxygen potential in their vicinity was lower for some other reason is uncertain at present. A thin continuous layer of Co_3O_4 was also found on the outside of scales, again formed on cooling. These features were also found in part with the higher chromium alloys.

Cobalt–20 and –30% Chromium

Scales on these two alloys usually spalled, often with sufficient violence to bend the specimen. This increase in residual compressive stress in the oxide with alloy chromium content probably indicated a decrease in stress relief by creep of the oxide (now Co–Cr spinel rich in its inner layers), or the alloy.

The scales on Co–20% Cr resembled those on Co–15% Cr, except that the alloy–oxide interface was extremely ragged (Fig. 7a), there being a very thin (2–4 μ) discontinuous layer of Cr_2O_3 (analyzed as 53.4% Cr because of its thinness) along this interface, but thicker at grain boundaries, with no band of internal oxide particles evident. Rarely was this layer continuous and totally protective, even when the total scale thickness was much less than elsewhere (Fig. 7b). The main body of the inner oxide layer after 50 hr exposure was two-phase, with horizontal bands (Fig. 7d), presumably of incorporated Cr_2O_3 partially converted to spinel (analyzed as 45.9 to 56.6% Cr). Few internal oxide particles were observed.

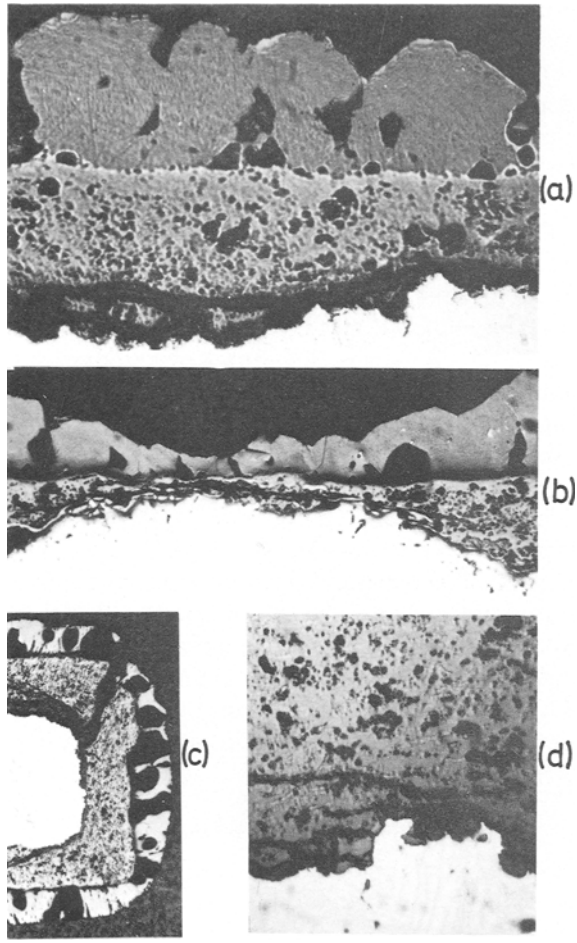

Fig. 7. Optical micrographs of scales formed on Co–20% Cr in 760 Torr oxygen at 1000°C. (a) 5 hr, ×500; (b) 25 hr, ×200; (c) 50 hr, ×60; (d) detail of alloy–oxide interface of (c), ×500. All parts reduced 20% for reproduction.

The oxide layers on the purer batch A Co–30% Cr were almost identical to those on Co–20% Cr, except that the inner major scale layer was always thicker than the outer layer (Fig. 8a). The outer CoO layer was relatively nonporous in some areas, while in others large holes, sometimes heavily decorated with Co_3O_4 as though molecular oxygen had penetrated them at temperature (Fig. 8a), were present. The thin Cr_2O_3 layer (analyzed as 61.0% Cr) at the alloy–oxide interface was always thicker than on Co–

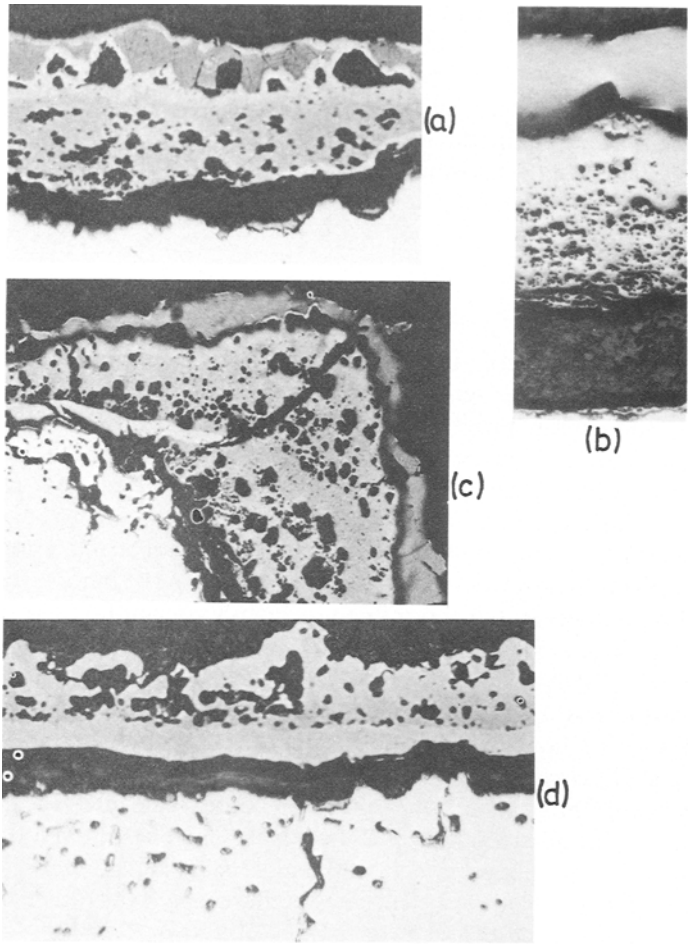

Fig. 8. Optical micrographs of scales formed on Co–30% Cr in 760 Torr oxygen at 1000°C. (a) Batch A, 5 hr, ×500; (b) batch A, 50 hr, ×200; (c) batch D, showing scale on a specimen corner, 240 hr, ×200; (d) batch D, 100 hr, ×500. All parts reduced 20% for reproduction.

20% Cr and apparently more continuous. The few internal oxide particles formed were associated with exposed alloy grain boundaries.

In contrast, the less pure batch D Co–30% Cr alloy surface was covered by a thin, relatively protective oxide (Fig. 8d) which had a major inner layer corresponding in composition to the $CoCr_2O_4$ spinel, beneath which was a thin layer of Cr_2O_3 (analyzed as 61.3% Cr) and above which was a layer of CoO. At specimen corners and in isolated random areas were patches of

thicker oxide, similar to those formed on batch A Co–30%Cr. One such area is shown in Fig. 8c, where part of the thin protective layer had been broken from the alloy surface and carried into the body of the scale. Probably these localized growths of thick scale were connected with the sudden sporadic increases in oxidation kinetics of this alloy, comparable to the limited scale breakaway described for a similar alloy by Davin *et al.*[3] In contrast with batch A Co–30%Cr, internal Cr_2O_3-rich oxide stringers were formed, the population of which increased with oxidation time.

Scale Analysis

With the exception of the point electron probe microanalysis of specific regions already quoted, interpretation of the many data obtained from scale sections of these alloys proved difficult. The cobalt and chromium traces for the thick inner oxide layers were extremely undulating and irregular, that for Co–15%Cr oxidized for 1 hr (Fig. 9a) being typical for the medium-chromium alloys. The internal oxide particles were too small to be resolved by the electron probe, so only a smeared-out chromium profile was possible for the particles themselves and those incorporated in the inner layer on the dilute alloys. However, the chromium was mainly concentrated in the inner scale layers, the chromium content of the outer layers always being low and near the limits of detection.

Ultraslow line scans through the part of the inner layer adjacent to the alloy (Figs. 9c–e) showed that as the alloy chromium content increased to 20 to 30% a slight chromium concentration gradient became apparent in the inner layer, chromium-lean at the inner scale–outer scale interface, together with a basal, chromium-rich layer 2–4 μ thick. The chromium levels (53.4 and 61.0%) for these layers on Co–20 and –30%Cr suggested Cr_2O_3, but sometimes it was difficult to be sure it was there as a layer rather than as a dense population of particles.

Little significant alloy chromium depletion occurred at the alloy–oxide interface for the Co–1 to –5%Cr alloys oxidized up to 5 hr but Co–10%Cr was depleted by 3.3% over 2 μ after 5 hr, and Co–15%Cr by 1% over 2 μ after 1 hr. Appreciable depletions occurred on the higher alloys, Co–20%Cr being depleted to 16.7% Cr over 5 μ after 5 hr, and batch A Co–30%Cr to 20.8% Cr over 15μ after 5 hr. After 100 hr, batch D Co–30%Cr showed a definite depleted band, 15 to 20 μ wide, where the chromium content had fallen to 25%.

As a means of comparing the oxides on the alloys, average chromium contents were determined for the inner layers by drawing the best horizontal straight line through each chromium profile, such that the total area under this line was the same as under the undulating profile. In general, neither the

average nor the peak chromium content of the inner layers changed much with increasing time for a given alloy, but both did increase with alloy chromium content (Table III). The leveling out of the average value at 39 to 43% Cr for alloys containing more than 15% Cr indicated that the inner layer closely approached the $CoCr_2O_4$-type structure, which has a theoretical chromium content of 45.9%. The finding of higher peak values in the depths of the inner layer must indicate incorporated Cr_2O_3, incompletely converted to $CoCr_2O_4$-type spinel. As expected, the average chromium level of the inner layer was lower at the specimen end than on the flat side.

In order to obtain a more quantitative analysis of the inner oxide layer, two specimens of Co–1% Cr were oxidized at 1200°C. A typical slow line scan across the inner layer showed that the internal oxide particles dissolved slowly upon incorporation into the scale, such that their apparent chromium contents were typically 25.9% directly upon incorporation, and 19.8%

Table III. Chromium Contents of the Oxide Layers Formed on Co–Cr Alloys in Oxygen at 1000°C

Alloy	Chromium content of outer (CoO) layers[a] Cr in CoO
Co–1% Cr	0 (1 hr), 0.06 (5 hr)
Co–2% Cr	< 0.2 (5 hr)
Co–5% Cr	0.16 (5 hr)
Co–5% Cr (Batch B)	0.3 (0.5 hr), 0.3 (1 hr), 0.1–0.2 (5 hr)
Co–10% Cr	0.4 (1 hr), 0.07 (5 hr)
Co–15% Cr	0.3 (1 hr)
Co–20% Cr	0.3 (5 hr)
Co–30% Cr (Batch A)	~0.3 (5 hr)

Alloy	Average chromium content of inner layers Average Cr level	Highest peak value
Co–1% Cr	3 (1 hr), 3 (5 hr)	4.5 (1 hr), 7.5 (5 hr)
Co–2% Cr	5 (5 hr), 3.5 (specimen end) (5 hr)	15.9 (5 hr)
Co–5% Cr	9.5 (1 hr)	27.8 (1 hr)
Co–5% Cr (Batch B)	9.0 (0.5 hr), 8.8 (1 hr), 9 (5 hr)	15.2 (0.5 hr), 14.8 (1 hr) 17.1 (5 hr)
Co–10% Cr	20.5 (1 hr), 19 (5 hr)	29.3 (1 hr), 32.7 (5 hr)
Co–15% Cr	31.8 (1 hr)	39.3 (1 hr)
Co–20% Cr	38 (5 hr)	53.4 (5 hr)
Co–30% Cr	43 (5 hr)	61 (5 hr)
Co–30% Cr (Batch D)	39 (100 hr)	61.3 (5 hr)

[a]These values in wt. % were determined at a distance of 20 μ from the interface with the inner layer.

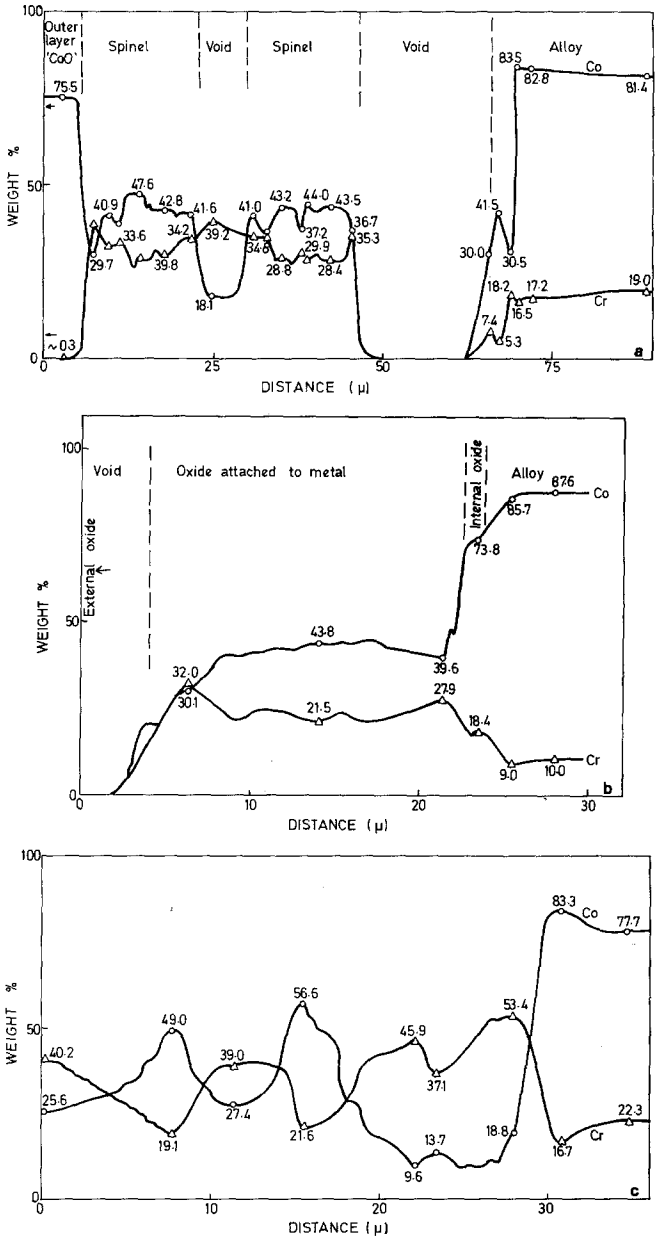

Fig. 9. Line scans with confirmed point analyses at the positions indicated, obtained from metallographic sections of Co–Cr alloys oxidized in 760 Torr oxygen, mainly at 1000°C. (a) Co–15%Cr, 1 hr; (b) Co–10%Cr, 5 hr, ultraslow scan through alloy–oxide interface; (c) Co–20%Cr, 5 hr, ultraslow scan through spinel layer.

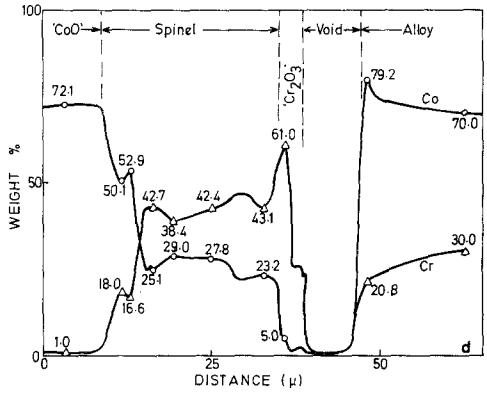

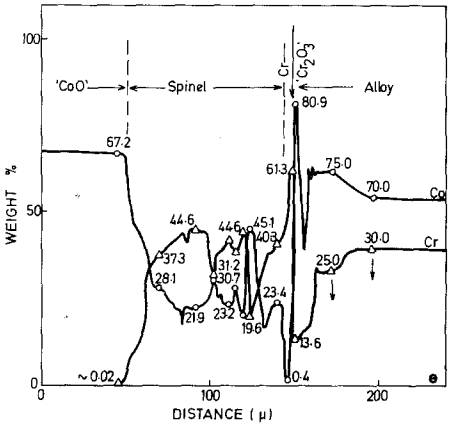

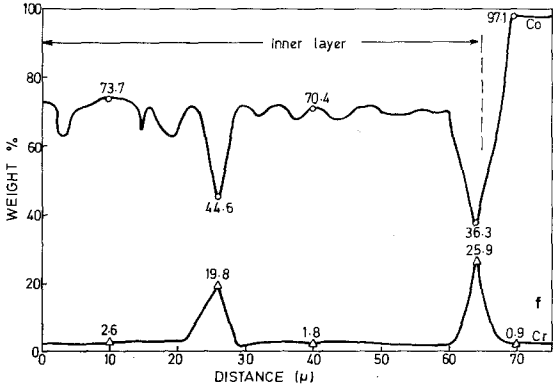

Fig. 9. Continued. (d) Batch A, Co–30%Cr, 5 hr; (e) batch D, Co–30%Cr, 100 hr (joined up internal oxide analyzes as Cr 64.7%, Co 0.6%); (f) Co–1%Cr, 2.5 hr, 1200°C.

when situated 30 μ into the inner layer (Fig. 9f). Although this trend may have been a particle size effect, the corresponding chromium content of the CoO rose from about 1.4–1.8% near the alloy–oxide interface to 2.6% deeper in the inner layer on both specimens. Because of the large interparticle spacing (20–30 μ) this value is thought to be an accurate measurement of the solubility of Cr^{3+} ions in CoO at 1200°C.

The chromium contents of the outer CoO layers formed on all the alloys were measured by line scans and spot analyses on the metallographically prepared cross sections. Although the possibility exists that smearing occurred during metallographic preparation, in the absence of such data gathered by other means we have listed in Table III the values measured 20 μ from the outer layer–inner layer interface, where effects due to fluorescence of chromium in the inner layer were considered to be minimal and from where the chromium level apparently remained the same to the outer edge of the oxide. No particular trend in the chromium level was evident, this being effectively constant at 0.2 to 0.4% Cr for the Co–2 and –30% Cr alloys, respectively. The value for Co–1% Cr was slightly lower, even after 5 hr.

Scale Layer Thicknesses

The excellent uniformity of the oxide layers enabled comparative thickness measurements to be made. These indicated that the rate indices for the increase of the total oxide thickness were the same as those obtained for the individual alloys from gravimetric measurements, cobalt and the Co–1 to –5% Cr alloys having values of n of 1.8 to 2.1, and Co–10 and –15% Cr giving values of 1.5 to 1.7. However, the outer CoO layers for cobalt and Co–1 to –15% Cr all grew parabolically (n = 1.9 to 2.2), whereas the inner layers grew faster than parabolically.

Some general trends are evident from Fig. 10, in which are plotted total thicknesses, inner and outer layer thicknesses, and total weight gains as functions of oxidation time and alloy chromium content. The total layer thicknesses were always greater on Co–1 to –15% Cr than on cobalt, and increased with alloy chromium content, becoming more pronounced with increased time. The outer layer thicknesses were slightly less on Co–1 to –15% Cr than on pure cobalt, and decreased slightly with increasing alloy chromium content, while the inner layer thicknesses were always greater than on cobalt and increased with alloy chromium content. The general shapes of the total oxide thickness and total weight gain curves were similar, but the trend of total scale thickness with chromium content was in some cases (Co–15% Cr after 1 and 2.5 hr) greater than the trend of weight gain with chromium content. This is thought to be an effect of porosity in the

scale. With alloys containing less than 15%Cr the outer oxide layer was thicker than the inner layer after all oxidation times studied, while with Co–15 and –20%Cr the inner layer became the thicker after longer than 5 hr. The differences in layer thicknesses on batch A Co–30%Cr increased markedly with time, the inner layer, however, always being thicker after all oxidation times.

DISCUSSION

Cobalt

Under the conditions studied, the essentially parabolic oxidation of cobalt appears controlled by the diffusion of Co^{2+} ions through a compact CoO layer. The formation of a fine-grained inner layer, thin along the specimen sides but thicker at the specimen ends, is more difficult to explain. The small grain size may, in part, be due to the concentration of impurities, particularly at the specimen ends, exerting a grain-refining effect and

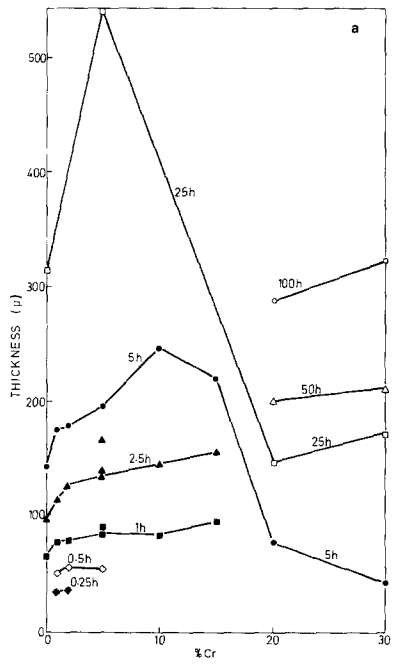

Fig. 10. Comparison of scale thicknesses and weight gains for Co–0 to 30%Cr alloys after different oxidation times. (a) Total scale thicknesses.

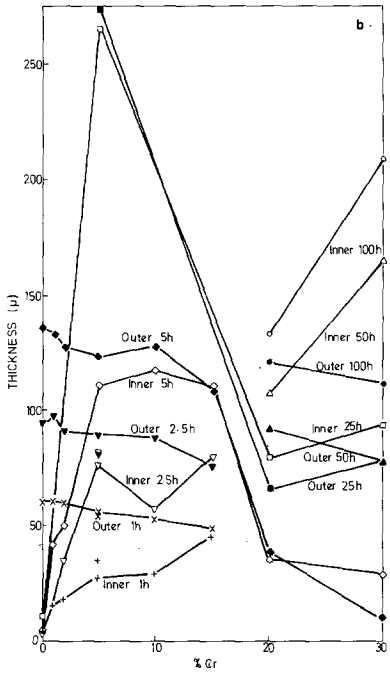

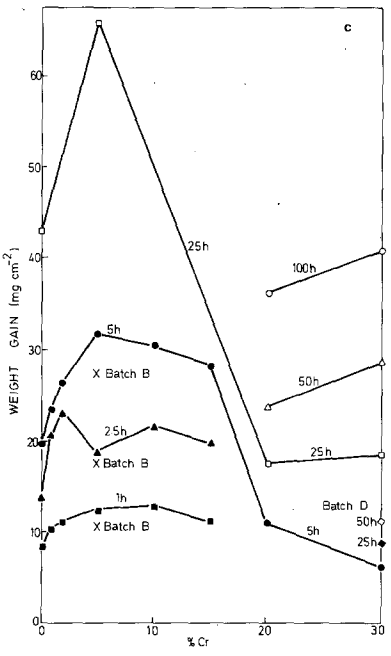

Fig. 10. Continued. (b) Inner and outer scale layer thicknesses; (c) total weight gains.

inhibiting creep, recrystallization, and grain growth, but this does not fully explain the continued contact between scale and receding metal there. Perhaps creep is sufficient to maintain contact, or else the rate of dissociation of CoO is sufficient to oxidize metal exposed by local scale–metal separation and eliminate gross void formation. The scale at the specimen corners is never more than 40% thicker than at the sides, despite the inner layer there approaching 70% of the total scale thickness. This tends to show that morphological differences in the scale do not have an overwhelming effect on oxidation kinetics at this temperature. Such enhancement in rate as there is presumably relates to dissociative transport of oxygen across the inner layer, or possibly enhanced grain-boundary diffusion of oxygen[16,17] or Co^{2+} ions[18] along oxide grain boundaries, as proposed for the corresponding NiO case.

Inward movement of oxygen through the outer layer by diffusion as ions,[17] or gas,[8] down columnar grain boundaries does not appear extensive, the precipitation of Co_3O_4 being no greater at specimen ends than on flat sides. There is no evidence of extensive perforation of the outer layer by anisotropic dissociation, or cracking, as found by Billman[8] for larger weight gains and higher temperatures. The Co_3O_4 particles in the outer CoO, in the CoO grain boundaries, and in the grain bodies are formed on cooling and indicate that the outer regions of the CoO are generally oxygen-rich at temperature. Little or no Co_3O_4 is found near the inner layer.

Consequently it seems most likely that scale tends to lose contact with the metal first at the ends, and particularly the corners, of the specimen. Oxygen is then supplied to the voids between the corner scale and the receding metal by dissociation of CoO further out in the scale, causing oxidation of the revealed metal and further porosity at its source. Scanning electron microscopy yields little supporting evidence for an interconnected network of voids, except perhaps close to the metal or a little further into the scale near the ends, but, as explained elsewhere,[11] interconnection of an array of pores is not required for dissociative transport of oxygen to contribute to scale growth.

Coldworking of the metal and different specimen thicknesses (although admittedly over a rather narrow range) had no effect on the oxidation rate, indicating that vacancy saturation effects in the metal and oxide grain size effects do not seem predominant under the present conditions.

Cobalt–1 to –15% Chromium

The overall control in oxidation of Co–Cr alloys containing up to 30% Cr is deduced to be the diffusion of ions through the total scale but with

different parts of it acting as the rate-determining region in various composition ranges, and with certain subsidiary processes occurring additionally.

Co–1 to –15%Cr alloys all oxidize faster than cobalt, usually conforming to a single, or occasionally two successive, parabolic regions. Figure 2 shows that a shallow curve can be drawn through the average parabolic rate constants for Co–2 to –15%Cr, while if the scatter of the rate constant values of individual specimens is included there is really little difference between Co–1%Cr and Co–2%Cr. This contrasts with earlier work,[2] where a sharp maximum in rate was found near Co–9%Cr.

In Fig. 8 only the outer layer thicknesses of the whole range of alloys Co–1 to –15%Cr are similar after most given oxidation times and, in fact, a trend for these layers to be slightly thinner with increasing alloy chromium content is evident. The outer scale layer also grows parabolically and these layers are only slightly thinner than the total scale on cobalt itself. There is thus some evidence that in this alloy range the outer scale layer is the predominant, largely rate-determining barrier to scale growth.

Nevertheless, it is instructive to compare the major differences between the scales on Co–2%Cr and C–15%Cr, which oxidized at almost identical rates.

a. The total scale thickness is always greater on Co–15%Cr.
b. The inner oxide layer is always much thicker on Co–15%Cr.
c. The outer oxide layers on both alloys are similar in thickness, that on Co–15%Cr being consistently slightly thinner after equivalent oxidation times.
d. A uniform thin band of densely packed internal oxide particles is present in Co–15%Cr.
e. The average chromium content of the inner oxide layer on Co–15%Cr is considerably higher (31.8%) than that on Co–2%Cr (5.0%), indicating a higher population density of Co–Cr spinel particles in the former case.
f. The chromium contents of the outer layers are similar (0.2–0.3% approximately) and are much less than in the inner layer (probably up to 1% at 1000°C if the figures of 1.6 to 2.6% at 1200°C are considered).

Clearly the total oxidation process is a complex one, with Co^{2+} transport across the entire scale being assisted by Cr^{3+} doping and inhibited by spinel and void presence in the inner layer, except that dissociative oxygen transport across these voids contributes to transport and effectively shortens the distance the Co^{2+} ions diffuse.[11] The evidence then seems to be that in the composition range Co–1 to –15%Cr the inner layer is effectively a short circuit and the outer layer largely determines the parabolic growth. Thus, the very thin band of Cr_2O_3 internal oxide and the spinel it becomes upon

incorporation determine the scale morphology to some degree, and influence the oxidation rate in this way, but they do not predominantly influence the rate directly by contributing to the total weight gain, or by forming blocking layers. Bearing in mind that spinel and internal oxide blocking and coalescence emerge as more important for Co–20 and –30% Cr, the nature of the inner layer is now considered in more detail.

Interplay of Spinel Blocking, Chromium Doping of CoO, and Porosity in the Inner Layer of Scales

The extrapolated diffusion coefficient[19,20] of Co^{2+} in $CoCr_2O_4$ at 1000°C is $1.7\times10^{-12}\,cm^2\cdot sec^{-1}$ and in $Co_{1.3}Cr_{1.8}O_4$ is $2.0\times10^{-13}\,cm^2\cdot sec^{-1}$. The corresponding figures for Cr^{3+} are 1.9×10^{-12} and $1.0\times10^{-13}\,cm^2\cdot sec^{-1}$. The diffusion coefficient[21] of Co^{2+} in undoped CoO is typically 2.6×10^{-9} to $4.1\times10^{-9}\,cm^2\cdot sec^{-1}$, which is approximately three orders of magnitude greater than in Co–Cr spinels. Spinel particles must therefore act as virtually complete blockages to outward Co^{2+} diffusion. That no slowing of the overall rate is effected by the inner layer on Co–15% Cr, where the average chromium content is 31.8%, is a little surprising at first sight. It must imply that dissociation transport of oxygen inwards and of Co^{2+} ions outwards through Cr^{3+}-doped CoO residual paths and any grain boundaries in the fine-grained material can quite readily keep up with Co^{2+} transport through the outer layer.

Whereas Cr^{3+} ions diffuse only slowly into the outer CoO, barely doping it, the CoO between the Co–Cr spinel particles in the inner layer eventually becomes saturated with Cr^{3+} ions. The solubility limit is about 2.6% Cr at 1200°C and, by analogy with the Ni–Cr system,[9] probably about 1% Cr at 1000°C. The extent of doping in the inner layer is therefore likely to be approximately constant for all alloys in the range Co–1 to –15% Cr but the spinel content increases with alloy chromium content. CoO has a considerably higher degree of natural stoichiometry than NiO,[9,21] so that doping effects by dissolved Cr^{3+} ions are less than with the more stoichiometric NiO and are clearly not great at the 1% Cr doping level.

Optical and scanning electron microscopy suggest that the outer columnar layers on Co–0 to –10% Cr are not very porous, while the inner layers are definitely porous in the immediate vicinity of the alloy–oxide interface and possibly through the entire inner layer thickness. In an attempt to assess the porosity of the scales, the total weight gain was plotted against the total scale thickness on the flat specimen sides for all specimens oxidized for different times, and the scale densities were calculated from the slopes.[12] In general, due to scatter and assumptions, it was not possible to come to any definite conclusions, except that the scale on the flat sides of cobalt seems essentially

nonporous (0.9% porosity). The present results tended to indicate that if it is assumed that the porosity is largely located in the inner layer it increases to a value of about 22% for Co–30%Cr. This does not compare particularly well with the results of Kofstad and Hed, who estimated 3–6% porosity in the outer layer and 33–35% porosity in the inner layer for scales on Co–10%Cr.

Dissociative transport has been considered in detail elsewhere.[9,11] Here it suffices to state that dissociation occurs in the inner layer and the inner regions of the outer layer but, as already indicated, there is no firm evidence of anisotropic dissociation of the outer layer rendering it open to the atmosphere for long periods. Another source of voids may be the coalescence of inward-flowing cation vacancies at second-phase particles in alloy or scale at or near the alloy–oxide interface. Dissociation of scale is enhanced by the demand of the alloy for oxygen to produce internal oxidation, which increases with alloy chromium content.[11] The internal oxide band is very thin in this case as it is rapidly encroached upon by the main scale. Probably the apparent increase in scale porosity with alloy chromium content is linked to the increasing importance of internal oxidation in enhancing dissociation of oxide in the surface scale.

These considerations support the earlier postulate that in the Co–1 to –15%Cr range rate control is predominantly through the barely doped outer CoO layer, since this would lead to a faster oxidation rate than with cobalt, and only requires the supply of Co^{2+} ions to the inner–outer scale interface to exceed the rate at which they can be transported through the outer layer.

Cobalt–20 and –30% Chromium

Although the alloys Co–20 and –30%Cr produce similar double-layered scales, with even thinner outer layers than the more dilute alloys, the slower oxidation rates of the alloys indicate that diffusion processes in the inner scale regions are rate-controlling. Batch A and batch D Co–30%Cr oxidize respectively at approximately $\frac{1}{3}$ and $\frac{1}{5}$ of the rate of cobalt. Now, the diffusion rate of Co^{2+} ions through Co–Cr spinel is at least three orders of magnitude less than through CoO. Consequently it appears that the rate-controlling process in the oxidation of these alloys is the diffusion of Co^{2+} ions through the few remaining CoO paths in a very spinel-rich inner layer (containing typically 38 and 39–43% Cr for Co–20%Cr and Co–30%Cr respectively). Clearly the inner layer cannot be completely spinel.

A densely packed layer of Cr_2O_3 particles forms as a thin layer at the alloy–oxide interface beneath the double-layered scale. However, it seems unlikely that this ever becomes completely continuous because the oxidation rates are several orders of magnitude faster than the rates when only Cr_2O_3 scales are formed.[2,3] In any case, transport through Cr_2O_3 occurs at

a roughly comparable rate to that through stoichiometric spinel. It is conceivable, however, that the diffusion through the tortuous oxide or alloy paths between the very densely packed band of Cr_2O_3 particles at the alloy–oxide interface could be rate-determining.

Batch D Co–30% Cr oxidizes slower than Batch A Co–30% Cr because of impurity effects promoting more complete Cr_2O_3 layer development, confirming Jones and Stringer,[14] who recently showed that Si additions to Co–Cr alloys assist Cr_2O_3 layer formation. Cr_2O_3 layer development can also be eased by oxidizing in a stagnant oxygen atmosphere in a deep crucible, i.e., effectively at a reduced oxygen potential.

CONCLUSIONS

1. The parabolic oxidation of cobalt in 760 Torr oxygen at 1000°C occurs predominantly by diffusion of Co^{2+} ions across a virtually pore-free columnar oxide. The very thin inner layer found on flat specimen sides and the thick inner layer at specimen ends probably grow by limited dissociation of the outer columnar CoO layer, possibly with some contribution from inward oxygen ion diffusion down grain boundaries, but the contribution to the total weight gain is rather small.

2. The outer CoO layers on Co–Cr alloys are relatively compact and contain no porosity of significance, there being no evidence of their complete perforation by anisotropic dissociation. They are always slightly thinner than corresponding layers on cobalt and contain at most 0.06 to 0.4% Cr towards their inner surfaces.

3. The total scale thicknesses on Co–1 to –15% Cr always exceed those on cobalt. The inner oxide layers contain particles of Co–Cr spinel, the population density of which increases with alloy chromium content. Some porosity definitely exists in inner layers next to the alloy surface, and it is likely that much of the inner layer is porous, possibly as a partially continuous network.

4. Internal oxidation of Co–Cr alloys is unimportant in the sense that it makes a negligible contribution to the weight gain, but it does help to determine the morphology and degree of porosity of the inner layers.

5. Doping of CoO in the outer layer by Cr^{3+} ions is minimal, but the chromium levels of the CoO in the fine-grained inner layer are greater, so doping is possible here, tending to increase the transport of Co^{2+} ions through the CoO.

6. Where basal layers of Cr_2O_3 or Co–Cr spinel are absent, the rate-determining step is the transport of Co^{2+} ions through CoO in the total scale layer, the weight gain responding to the complex interaction of doping of CoO by Cr^{3+} ions, void and spinel blockage of cation transport in the

inner layer and dissociative transport of oxygen across pores in the inner layer. The last effect satisfies the tendency of chromium to oxidize in a fine band slightly ahead of the rapidly advancing main scale. The greatest impediment to Co^{2+} diffusion may well be the outer layer for dilute alloys, where the inner layer is doped and porous but, for alloys richer in chromium, it is probably diffusion through a convoluted CoO path between a high population density of Co–Cr spinel particles in the inner layer.

7. The coalescence of Co–Cr spinel particles to give a complete layer may be approached in the Co–15 to –30% Cr alloys, slowing the oxidation rate, but eventual scale healing is by a thin Cr_2O_3 layer which tends to form at the scale base for Co–20 to –30% Cr. This layer is tenuous and difficult to form for purer alloys, but in lower oxygen potentials or with impurer alloys its establishment is facilitated.

8. To make a complex situation even more involved, it must be recognized that overheating, scale cracking (possibly evidenced by discontinuities in the weight gain-time curves, banding of the spinel in the inner layer, and more rapid scale growth on the specimen ends), and scale perforated by anisotropic oxide dissociation (possibly hinted at here in the inner regions of columnar grain boundaries and at the scale ends) may be more important in more extreme conditions and lead to direct oxygen gas access to the alloy. Clearly this would lead to more enhanced oxidation than the alternative possibility of O^{2-} ion diffusion down the columnar grain boundaries. The inner layer becomes very fine grained for the more chromium-rich alloys, which may mean that inward O^{2-} ion diffusion and outward Co^{2+} diffusion along grain boundaries assist doping and dissociation oxygen transport in providing transport in the inner layers.

ACKNOWLEDGMENTS

We are indebted to the Science Research Council for supporting one of the authors from 1967 to 1969 when this work was undertaken, and to various organizations for supplying alloys.

REFERENCES

1. A. Preece and J. Lucas, *J. Inst. Met.* **81**, 219 (1952).
2. C. A. Phalnikar, E. B. Evans, and W. M. Baldwin, *J. Electrochem. Soc.* **103**, 429 (1956).
3. A. Davin, D. Coutsouradis, and L. Habraken, *Cobalt* **35**, 69 (1967).
4. A. S. Tumarev and S. N. Sumin, *Fiz. Met. Metallov*, ed. Trudy LP1, **305**, 92 (1970).
5. P. K. Kofstad and A. Z. Hed, *J. Electrochem. Soc.* **116**, 224, 229, 1542 (1969).
6. P. K. Kofstad and A. Z. Hed, *Oxid. Met.* **2**, 101 (1970).
7. P. K. Kofstad and A. Z. Hed, *Werkst. Korros.* **21**, 895 (1970).
8. F. R. Billman, *J. Electrochem. Soc.* **119**, 1198 (1972).
9. G. C. Wood, I. G. Wright, T. Hodgkiess, and D. P. Whittle, *Werkst. Korros.* **21**, 900 (1970).

10. I. G. Wright, "Oxidation of Iron-, Nickel- and Cobalt-Base Alloys," Metals and Ceramics Information Center, Battelle-Columbus Laboratories, Rep. MCIC-72-07 (June 1972).
11. F. H. Stott, I. G. Wright, T. Hodgkiess, and G. C. Wood, *Oxid. Met.* **11**, 141 (1977).
12. I. G. Wright, Ph.D. Thesis, University of Manchester (1969).
13. G. N. Irving, J. Stringer, and D. P. Whittle, *Oxid. Met.* **8**, 393 (1974).
14. D. E. Jones and J. Stringer, *Oxid. Met.* **9**, 409 (1975).
15. G. C. Wood and T. Hodgkiess, *J. Electrochem. Soc.* **113**, 319 (1966).
16. J. Kruger, A. Melin, and H. Winterhagen, *Cobalt* **33**, 176 (1966).
17. F. N. Rhines and J. S. Wolf, *Metall. Trans.* **1**, 1701 (1970).
18. D. Caplan, M. J. Graham, and M. Cohen, *J. Electrochem. Soc.* **119**, 1205 (1972).
19. R. Sun, *J. Chem. Phys.* **28**, 290 (1958).
20. A. Morkel and H. Schmalzried, *Z. Phys. Chem.* **32**, 76 (1962).
21. N. G. Eror and J. B. Wagner, *J. Phys. Chem. Solids* **29**, 1597 (1968).